Contact Angle of the Colloidal Liquid-Gas Interface and a Hard Wall

Paul P. F. Wessels*
Institut für Theoretische Physik II, Heinrich-Heine-Universität Düsseldorf, Universitätsstraße 1, 40225 Düsseldorf, Germany

Matthias Schmidt†
Debye Institute, Utrecht University, Princetonplein 5, 3584 CC Utrecht, The Netherlands

Hartmut Löwen
Institut für Theoretische Physik II, Heinrich-Heine-Universität Düsseldorf, Universitätsstraße 1, 40225 Düsseldorf, Germany

(Dated: 6 May 2004)

We consider the Asakura-Oosawa-Vrij model of hard sphere colloids and ideal polymer coils in contact with a planar hard wall at (colloidal) liquid-gas coexistence. Using extensive numerical density functional calculations, the liquid-gas, wall-liquid and wall-gas interfacial free energies are calculated. The results are inserted into Young's equation to obtain the contact angle between the liquid-gas interface and the wall. As a function of polymer fugacity this angle exhibits discontinuities of slope ("kinks") upon crossing first-order surface phase transitions located on the gas branch of the bulk binodal. Each kink corresponds to a transition from $n-1$ to n colloid layers adsorbed at the wall, referred to as the n'th layering transition. The corresponding adsorption spinodal points from $n-1$ to n layers upon reducing the polymer fugacity along the bulk binodal were found in a previous study (J. M. Brader et al. J. Phys.: Cond. Matt., 14: L1, 2002; Mol. Phys., 101: 3349, 2003). Remarkably, we find desorption spinodal points from n to $n-1$ layers to be absent upon increasing polymer fugacity at bulk coexistence, and many branches (containing up to 7 colloid layers) remain metastable. Results for the first layering binodal and both spinodal branches off-bulk coexistence hint at a topology of the surface phase diagram consistent with these findings. Both the order of the transition to complete wetting and whether it is preceded by a finite or an infinite number of layering transitions remain open questions. We compare the locations of the first layering binodal line and of the second layering binodal point at bulk coexistence with recent computer simulation results by Dijkstra and van Roij (Phys. Rev. Lett., 89: 208303, 2002) and discuss our results for the contact angle in the light of recent experiments.

I. INTRODUCTION

In suspensions of sterically-stabilized colloidal particles mixed with nonadsorbing globular polymers, the latter induce an effective attraction between the colloids due to the depletion effect [1]. Such mixtures can phase separate into two fluid phases, one being a colloidal liquid that is rich in colloids and poor in polymers and the other being a colloidal gas that is poor in colloids and rich in polymers. Colloid-polymer mixtures serve as excellent model systems to study many phenomena associated with liquid-gas phase separation as time and length scales are much larger than in atomic and molecular systems [1, 2]. Recent experiments have focused on the bulk phase behaviour [1] (and Refs. therein), (colloidal) liquid-gas interface tension [3, 4, 5, 6, 7], capillary wave fluctuations observed in real space [8], droplet coalescence [8] and further non-equilibrium phenomena [1, 7, 9]. The behaviour at nonadsorbing walls has been studied by measuring the contact angle between the free liquid-gas interface and a substrate acting as a hard wall. Complete wetting of the wall by the colloidal liquid has been observed for a wide variety of statepoints [9]. However, there are also reports of a transition from partial to complete wetting [10, 11], hence this remains an interesting topic.

Most of the essential physics of colloid-polymer mixtures is captured by the Asakura-Oosawa-Vrij (AO) model of hard-sphere colloids and ideal polymers [12, 13, 14], and which has become a widely-used reference system. Theoretical approaches [15, 16] and computer simulations [17, 18, 19, 20, 21, 22, 23] have given insight into its bulk phase behaviour, and some recent work [20, 24] aims at including more realistic colloid-polymer and polymer-polymer interactions. Studies based on a one-component description of colloids interacting with an effective depletion potential (obtained by integrating out the polymer degrees of freedom and truncating at the pair-wise level) were devoted to inhomogeneous situations, such as the free fluid-fluid interface [25, 26] and adsorption at a hard wall [27]. Following the development of an accurate density functional theory (DFT) specific for the binary AO model [28, 29], further research was stimulated in inhomogeneous situations such as liquid-gas [30, 31] and wall-fluid interfaces [30, 31, 32] and results were compared to those from

*Electronic address: wessels@thphy.uni-duesseldorf.de
†On leave from: Institut für Theoretische Physik II, Heinrich-Heine-Universität Düsseldorf, Universitätsstraße 1, 40225 Düsseldorf, Germany

simulations [21, 22, 23, 33]. In particular, in Refs. [30, 31] the AO model was considered in contact with a planar hard wall. A sequence of first-order layering transitions was found on the gas branch of the (liquid-gas) binodal upon reducing the polymer fugacity. Further reducing the polymer fugacity leads to a transition to complete wetting of the wall by colloidal liquid. This scenario was corroborated by a simulation study [21]. The relation of the results from these different approaches will be reexamined in the light of the findings of the present study in more detail below. The adsorption properties at a wall are intimately related to the wall-fluid interfacial free energies (or "wall tensions"), for which an analytical expression was obtained from a scaled-particle treatment and which was found to compare well with results from full numerical DFT calculations [32]. However, despite its experimental accessibility [7, 9, 10, 11], the contact angle of the free liquid-gas interface and a hard planar wall has not been considered neither by theory nor simulations, in contrast to wetting behavior [21, 30, 31, 34]. The aim of the present study is to obtain a quantitative understanding of the contact angle and elucidate its relation to the surface phase behavior on the basis of the AO model.

We obtain the (macroscopic) contact angle, θ, from the liquid-gas (lg), the wall-gas (wg) and the wall-liquid (wl) interface tensions, γ_{lg}, γ_{wg} and γ_{wl}, respectively, via Young's equation [35],

$$\cos\theta = \frac{\gamma_{wg} - \gamma_{wl}}{\gamma_{lg}}. \quad (1)$$

A similar depletion attraction that acts between two colloids acts between one colloid and a hard wall [27]; the latter therefore favours the colloidal liquid. As a consequence, we expect $\gamma_{wg} > \gamma_{wl}$ everywhere at coexistence, and $\theta < \pi/2$. For statepoints where $\gamma_{wg} < \gamma_{wl} + \gamma_{lg}$, the contact angle $\theta > 0$ and the surface is partially wet by the liquid. However, as soon as $\gamma_{wg} = \gamma_{wl} + \gamma_{lg}$ a macroscopic liquid layer will intrude between the gas and the wall and the latter is completely wet by the liquid. The transition from partial to complete wetting induced by changing an appropriate thermodynamic variable is referred to as the wetting transition [36, 37]. A study of θ can supply a link between theoretical predictions of surface phase behavior and experiments and we display our central result in Fig. 6.

The paper is organized as follows, in Sec. II we define the model and and discuss in Sec. III the density functional theory used to calculate the interface tensions. In Sec. IV we present results and we conclude in Sec.V.

II. MODEL

We consider the Asakura-Oosawa-Vrij (AO) model of N_c hard-sphere colloids and N_p ideal polymers in a volume V. The colloids (species c) and polymers (species$p$) have diameters σ_i, bulk packing fractions $\eta_i = N_i V_i/V$, and particle volumes $V_i = (\pi/6)\sigma_i^3$ for $i = c, p$, respectively. The colloid-colloid as well as the colloid-polymer interaction potentials are those of hard spheres, so $u_{ij}(r) = \infty$ when $r < (\sigma_i + \sigma_j)/2$ and $u_{ij}(r) = 0$ otherwise, with $ij = cc, cp$. The polymers do not interact with each other, i.e. $u_{pp}(r) = 0$ for all r. Due to the non-additive ranges of these interaction potentials, the polymers induce an effective attraction between the colloids, which for sufficiently large size ratios σ_p/σ_c ($\gtrsim 0.35$) drives a thermodynamically stable phase separation into a colloid-rich (liquid) and a colloid-poor (gas) phase [15, 16]. All bare interactions are of an entropic nature, and therefore the temperature T does not play a role. The only relevant model parameter is the size ratio $q = \sigma_p/\sigma_c$. We often use the so-called polymer-reservoir representation where the mixture is in contact with a polymer reservoir, which determines the polymer chemical potential. In this situation, the thermodynamic state parameters are η_c and η_p^r, the latter being the polymer packing fraction in the reservoir which is proportional to the polymer fugacity as these particles are ideal.

III. DENSITY FUNCTIONAL THEORY

We use the fundamental measure density functional for the AO model [28, 29] to calculate colloid and polymer density profiles from which the interface tensions can then be obtained. In density functional theory (DFT), the grand-canonical free energy is expressed as a functional, $\Omega[\rho_c(\mathbf{r}), \rho_p(\mathbf{r})]$, of the one-particle distribution functions $\rho_i(\mathbf{r})$ (with $i = c, p$), given by [38]

$$\begin{aligned}\Omega[\rho_c(\mathbf{r}), \rho_p(\mathbf{r})] &= F_{\rm exc}[\rho_c(\mathbf{r}), \rho_p(\mathbf{r})] \\ &+ k_{\rm B}T \sum_{i=c,p} \int d\mathbf{r}\rho_i(\mathbf{r}) \left[\ln\left(\rho_i(\mathbf{r})\Delta_i\right) - 1\right] \\ &+ \sum_{i=c,p} \int d\mathbf{r}\rho_i(\mathbf{r}) \left[u_{{\rm ext},i}(\mathbf{r}) - \mu_i\right], \quad (2)\end{aligned}$$

where $k_{\rm B}$ is Boltzmann's constant, Δ_i is the "thermal volume" of species i, i.e. the third power of the de Broglie wave length, and $u_{{\rm ext},i}(\mathbf{r})$ and μ_i are the external potential and the chemical potential for species i, respectively. The excess Helmholtz free energy functional, $F_{\rm exc} = \int d\mathbf{r}\Phi(\mathbf{r})$, with Φ the excess free energy density, is given in Refs. [28, 29] and is not reproduced here [47].

In thermodynamic equilibrium, the functional is stationary, $\delta\Omega/\delta\rho_i(\mathbf{r}) = 0$ (with $i = c, p$), and the resulting equations yield the stable distributions, i.e.

$$\rho_i(\mathbf{r}) = z_i \exp\left[-\beta u_{{\rm ext},i}(\mathbf{r}) - \beta\frac{\delta F_{\rm exc}[\{\rho_j(\mathbf{r})\}]}{\delta\rho_i(\mathbf{r})}\right], \quad (3)$$

with $z_i = \Delta_i^{-1}\exp[\beta\mu_i]$ the fugacity of component i and $\beta = 1/k_{\rm B}T$. The equilibrium distribution functions are normalized, $\int d\mathbf{r}\rho_i(\mathbf{r}) = N_i$. We note that the polymer fugacity is proportional to the polymer packing fraction

in the polymer reservoir, $\eta_p^r = z_p V_p$, and we usually refer to η_p^r as the polymer fugacity. We have solved these equations numerically for $\rho_i(z)$ in one spatial dimension z for the free liquid-gas interface (where $u_{\mathrm{ext},i}(z) = 0$ everywhere) as well as both for the liquid and the gas at bulk coexistence in the presence of the external hard-wall potential, i.e. for $u_{\mathrm{ext},i}(z) = \infty$ for $z < \sigma_i/2$ and $u_{\mathrm{ext},i}(z) = 0$ otherwise for both species $i = c, p$, where z is the space coordinate perpendicular to the wall. The numerical routine we have used is a Picard iteration procedure with a Broyles mixing scheme [39]. The "mixing parameter" is continuously adapted to obtain optimal convergence. Additionally, it is important to realize that in situations with several metastable minima, as we find to occur for the coexisting gas in contact with the hard wall, the initial guess for the profiles in the iteration procedure determines to which minimum the routine converges.

Once the density profiles are known, the interface tension is given by $\gamma = (\Omega_{\mathrm{inh}} + PV)/A$, where $\Omega_{\mathrm{inh}} = \Omega[\rho_c(\mathbf{r}), \rho_p(\mathbf{r})]$ (i.e. the functional, Eq. 2, evaluated at the solutions of Eq. 3) is the grand-canonical free energy of the inhomogeneous system, P is the bulk pressure, and A is the lateral (perpendicular to the z-direction) system area. In terms of density profiles this quantity can be written as

$$\gamma = \int dz \left[\omega(z) + P\right], \tag{4}$$

where

$$\omega(z) = k_{\mathrm{B}}T \sum_{i=c,p} \rho_i(z) \left[\ln\left(\rho_i(z)\Delta_i\right) - 1\right] - \sum_{i=c,p} \mu_i \rho_i(z) + k_{\mathrm{B}}T\Phi(z) \tag{5}$$

can be viewed as a local grand potential density (evaluated with the minimized density profiles). In case of the liquid-gas interface, the integral in Eq. 4 is over all space, i.e. z runs from $-\infty$ (bulk gas) to ∞ (bulk liquid). In case of the fluid in contact with a hard wall, the integral runs from $z = 0$ (at the actual location of the hard wall) to ∞ (bulk). In the numerical routine, we compute the interface tensions for each statepoint for different system sizes and refined termination criteria for the iteration. This gives an estimate of the numerical error in the result for the interface tensions, which is important as the resulting contact angle can be very sensitive to these errors. Often the dividing surface [35] is chosen at $z = \sigma_c/2$; then subtraction of $\sum_{i=c,p} P\sigma_i$ from the present definition of the wall-fluid tension, Eq. 4, is required. For our present goal this is irrelevant as this term does not affect θ, as it drops out of the numerator in Eq. 1.

IV. RESULTS

A. Layered states at the hard wall

We have calculated colloid and polymer density profiles of the free liquid-gas interface, as well as the wall-gas and the wall-liquid interfacial profiles at bulk coexistence. For a given statepoint the liquid-gas and the wall-liquid profiles are both unique (disregarding trivial translations of the liquid-gas interface); such results have been presented elsewhere [30, 31]. However, in case of the coexisting gas in contact with the hard wall, we have found many metastable states, each corresponding to an integer number of layers, n, of colloids adsorbed at the wall. In Figs. 1 and 2, we have plotted a number of such profiles, denoted by $\rho_{c,n}(z)$, for size ratio $q = 0.6$ and fugacities $\eta_p^r = 1.2$ and $\eta_p^r = 0.8$, respectively, along with the corresponding polymer profiles, $\rho_{p,n}(z)$, given in the respective insets (for reference, the bulk phase diagram for $q = 0.6$ is given in the inset of Fig. 9). For $\eta_p^r = 1.2$ the 0-layer state (marked with an asterisk in Fig. 1) exhibits practically no excess colloid adsorption and is the globally stable state. The grand potential and hence the interface tension increases with the number of layers, i.e. $\gamma_{wg,0} < \gamma_{wg,1} < \gamma_{wg,2} < \ldots < \gamma_{wg,7}$, where $\gamma_{wg,n}$ is the wall-gas tension corresponding to n colloid layers (as given in Eq. 4 and evaluated with $\rho_{i,n}(z), i = c, p$). For $\eta_p^r = 0.8$ the equilibrium profile is given by $\rho_{i,1}(z)$ (marked with an asterisk in Fig. 2). Remarkably, in this case, the solution $\rho_{i,0}(z)$ corresponds to a higher tension than all others, i.e. $\gamma_{wg,1} < \gamma_{wg,2} < \ldots < \gamma_{wg,6} < \gamma_{wg,0}$. The two state points considered ($\eta_p^r = 0.8, 1.2$) are at polymer fugacities larger than that at which the Fisher-Widom line [40, 41] hits the bulk binodal (at $\eta_p^r \approx 0.533$ for $q = 0.6$ [29]), which implies that correlations decay asymptotically in an oscillatory fashion in the liquid phase. Apparently, this oscillatory nature also appears in the effective interface potential between wall and the liquid-gas interface, yielding many metastable minima [31], see Refs. [42].

B. Wall contact angle of the liquid-gas interface

We have calculated the liquid-gas interface tension, γ_{lg}, the wall-liquid tension, γ_{wl}, and the wall-gas tensions for all n-layer states identified, $\gamma_{wg,n}$, for the full range of polymer fugacities at bulk liquid-gas coexistence. The results have been inserted into Young's equation, Eq. 1, yielding a contact angle curve, θ_n, for each n-layer state. The results for $q = 0.6$ are plotted in Fig. 3 and a magnification of the region close to $\cos\theta_n = 1$ is displayed in Fig. 4. From the definition of the contact angle, Eq. 1, and the fact that γ_{lg} and γ_{wl} are unique for each statepoint, η_p^r, the state n with the lowest free energy also possesses the lowest value of $\cos\theta_n$. Hence, for high η_p^r the *equilibrium* contact angle is given by θ_0 (corresponding to the 0-layer state), see Fig. 3. Decreasing η_p^r,

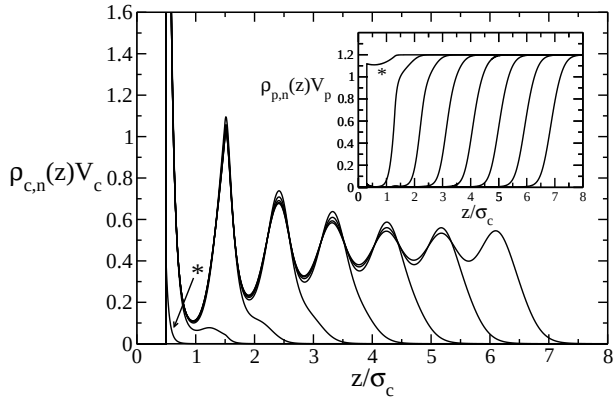

FIG. 1: Colloid density profiles, $\rho_{c,n}(z)V_c$, at a hard wall as a function of the scaled distance, z/σ_c, from the wall at the gas branch of liquid-gas binodal for $q = 0.6$ and $\eta_p^r = 1.2$. Shown are results for n-layer states with $n = 0, 1, 2, \ldots, 7$ (left to right). All states are metastable except for the globally stable $n = 0$-layer state (see the small peak at contact with the wall, marked with an asterisk). The inset shows the corresponding polymer profiles (also from left to right, with asterisk marking $n = 0$-layer state), $\rho_{p,n}(z)V_p$, as a function of z/σ_c. The normalizations of the density profiles are such that in bulk they reduce to the packing fractions, $\lim_{z\to\infty} \rho_{i,n}(z)V_i = \eta_i$.

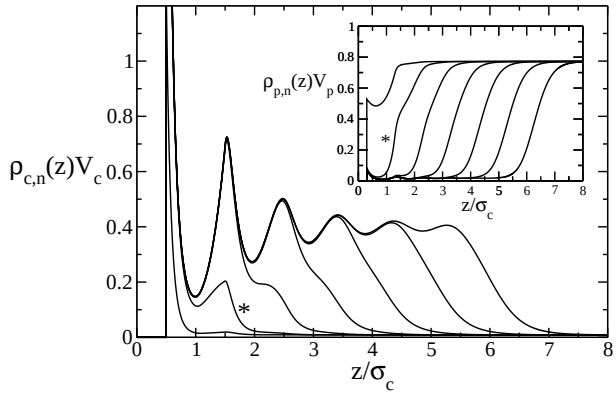

FIG. 2: Same as Fig. 1, but for $\eta_p^r = 0.8$ and $n = 0, 1, 2, \ldots, 6$ (left to right). All profiles are metastable except for the globally stable $n = 1$-state (marked with asterisks).

leads to an increase in $\cos\theta_0$, until it crosses the $\cos\theta_1$ branch, and becomes metastable. The crossing point, where $\theta_0 = \theta_1$, denotes the 0-1 layering transition and is also referred to as the *first* layering transition. (Consistent with Refs. [30, 31], the surface phase transition from $n-1$ to n adsorbed colloid layers at the wall-gas interface is referred to as the n'th layering transition.) Upon further decreasing η_p^r (see Fig. 4), $\cos\theta_1$ is in turn crossed by $\cos\theta_2$ and the crossing point, where $\theta_1 = \theta_2$, is the 1-2 (second) layering transition. This scheme suggests that there could well be further layering transitions upon reducing η_p^r, and this impression is strengthened by the fact that the (metastable) states $\cos\theta_n$ (with n from 3 to 7, see Fig. 4), all seem to converge to around the location of the wetting transition. However, we have not been able to resolve the third [30, 31] and (possible) higher layering transitions and we note that any of these should be located in the small region of $\cos\theta$ between 0.995 and 1 with η_p^r between 0.6 and 0.65, see Fig. 4. Consequently, we can also not obtain insight into the nature of the transition to complete wetting, i.e. whether this is second-order and occurs via an infinite sequence of layering transitions or it is first order and is preceded by only a finite number of layering transitions. For a more extensive discussion of these two possible scenarios, we refer the reader to Ref. [31].

Upon reducing η_p^r, metastable 0-layer states can be tracked into a region where the contact angle takes unphysical values, $\cos\theta_0 > 1$ (Fig. 3). The same happens for 1-layer states as can be seen in Fig. 4. Inserting equilibrium values of the interface tensions obtained from DFT into Eq. 1 ensures that $\cos\theta \leq 1$, but this does not need to be the case when using interface tensions of metastable states. Reducing η_p^r even further, the metastable 0-layer state eventually becomes unstable at an adsorption spinodal point, see Fig. 3. Beyond this point (for even lower η_p^r), no 0-layer state can be stabilized and the numerical iteration rather converges to the 1-layer state. Similar adsorption spinodal points were found for higher n and we have located those with a (moderate) resolution of 0.05 in η_p^r. ¿From the present data the adsorption spinodal fugacities for n-layer states, $\eta_{p,n'}^r$, are $\eta_{p,0'}^r = 0.75$, $\eta_{p,1'}^r = \eta_{p,2'}^r = 0.65$ and $\eta_{p,3'}^r = \eta_{p,4'}^r = \eta_{p,5'}^r = 0.6$. For states with an even thicker colloid film ($n = 6$ and 7), the profiles no longer converged properly at low η_p^r, and we can have not been able to obtain precise values for $\eta_{p,6'}^r$ and $\eta_{p,7'}^r$. The evolution for surface states upon *increasing* η_p^r is in striking contrast. No spinodal points were found and each n-layer state remains metastable up to $\eta_p^r = 1.5$, a value close to the liquid-gas-crystal triple point according to free-volume-theory for the AO model [16]. Moreover, for large values of η_p^r the numerical routine converges very rapidly, which hints at deep (nevertheless metastable) free-energy minima for these layered surface states.

As the layering transitions are thermodynamic surface phase transitions, they manifest themselves as discontinuous jumps in the Gibbs adsorption [30, 31],

$$\Gamma_i = \int_0^\infty \mathrm{d}z(\rho_i(z) - \rho_i(\infty)), \tag{6}$$

for both components $i = c, p$, and these can be obtained from Eq. 5 and

$$\Gamma_c = -\left.\frac{\partial\gamma_{wf}}{\partial\mu_c}\right|_{\mu_p}, \quad \Gamma_p = -\left.\frac{\partial\gamma_{wf}}{\partial\mu_p}\right|_{\mu_c}, \tag{7}$$

where γ_{wf} is the wall tension of the fluid. Moving along the gas branch of the liquid-gas bulk binodal ties together changes in both chemical potentials:

$$\left.\frac{d\gamma_{wg}}{d\mu_p}\right|_{\mathrm{coex}} = \left.\frac{\partial\gamma_{wg}}{\partial\mu_p}\right|_{\mu_c} + \left.\frac{\partial\gamma_{wg}}{\partial\mu_c}\right|_{\mu_p} \left.\frac{d\mu_c}{d\mu_p}\right|_{\mathrm{coex}}, \tag{8}$$

where the slope of the bulk binodal fulfills a Clapeyron-type equation,

$$\left.\frac{d\mu_c}{d\mu_p}\right|_{\rm coex} = -\frac{\Delta\rho_p}{\Delta\rho_c}, \tag{9}$$

which can be deduced from the Gibbs-Duhem equation in a straightforward fashion [43]. Here, $\Delta\rho_i = \rho_i^l - \rho_i^g$ is the difference in density of species $i = c, p$ in the liquid and in the gas phase (note that $\Delta\rho_p < 0$). Hence, we obtain

$$\left.\frac{d\gamma_{wg}}{d\mu_p}\right|_{\rm coex} = -\Gamma_p + \Gamma_c\frac{\Delta\rho_p}{\Delta\rho_c}, \tag{10}$$

where the adsorptions Γ_c and Γ_p refer to those of the gas at bulk coexistence. Hence, as crossing a layering transition (again at bulk coexistence) is necessarily accompanied by a jump in the adsorptions Γ_i, consequently via Eq. 10 this leads to a discontinuity of slope of the wall-gas interface tension. ¿From Young's equation 1, it follows that this also leads to a jump in the slope of the contact angle, $d\cos\theta/d\eta_p^r$. This is consistent with our findings above of crossing of different branches, θ_{n-1} and θ_n [48].

Note that all quantities in Eq. 10 can be independently obtained from our DFT results, namely the adsorption Γ_i from the integral over the respective density profile, Eq. 6, the differences $\Delta\rho_i$ from the bulk phase diagram, and the left hand side of Eq. 10 from a numerical derivative of the results for γ_{wg}, as obtained through Eq. 4. As a check for internal consistency of our calculations we have chosen the statepoint with $\eta_p^r = 1.1$ for $q = 1$ at bulk coexistence, which is very close to the binodal of first layering transition (which is at $\eta_p^r \approx 1.104$, as discussed below). We find Eq. 10 to be fulfilled to three significant digits; for the 0-layer (1-layer) state either sides evaluate to $1.264/\sigma_c^2$ ($1.352/\sigma_c^2$). Together these two estimates yield a jump in $d\cos\theta/d\eta_p^r$ of 0.247, which is consistent with our data for the contact angle for $q = 1$ (which gives 0.238) and which is discussed below.

We will now consider the case of larger polymer-colloid size ratios, $q = 1$, see Fig. 5 in more detail. The 0-layer branch is calculated for a number of fugacities from high values, $\eta_p^r = 3$, to the spinodal point close to $\eta_p^r = 1$. The higher-n branches are only calculated between 0.95 and 1.5 ($n = 1$) and between the wetting transition [31] and the crossing point of the 0-layer and the 1-layer branch ($n = 2-6$, which practically fall on top of each other). It is found that for this size ratio the 0-layer branch is the stable everywhere except in a small regime of η_p^r between 0.85 and 1.1 (where $\cos\theta_n$ is close to 1) and where layering transitions are located. We have been able to identify the locations of the first and second layering transitions, higher transitions are eroded by the numerical noise.

Fig. 6 shows the resulting equilibrium values of $\cos\theta$ (see the inset for the bare angle θ) as a function of the difference in colloid packing fractions of the coexisting liquid and gas phases, $\eta_c^l - \eta_c^g$, for both size ratios considered, $q = 0.6$ and $q = 1$. This representation enables one to make direct contact with experiments, where density differences of coexisting phases are rather directly accessible [7, 9, 10, 11]. For both size ratios the contact angle is of the same order of magnitude, i.e. $\cos\theta = 0.8 - 1$, but for $q = 1$ the wetting transition lies closer (in this representation) to the bulk critical point. Only the first layering transition for $q = 0.6$ occurs at a considerably large contact angle of $\cos\theta_{0-1} \approx 0.95$ or $\theta_{0-1} \approx 18^{\rm o}$. A

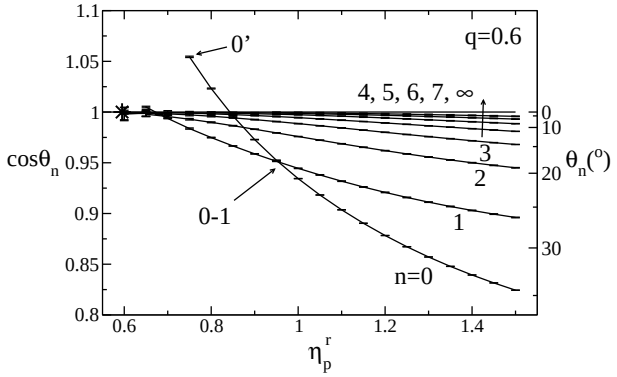

FIG. 3: Cosines of the contact angle, $\cos\theta_n$ as defined via Young's equation as $(\gamma_{wg} - \gamma_{wl})/\gamma_{lg}$, as a function of the polymer reservoir packing fraction, η_p^r, for size ratio $q = 0.6$. A scale of the bare angle (in degrees, °) is given on the right vertical axis. Shown are branches, θ_n, corresponding to n colloid layers adsorbed at the wall-gas interface at liquid-gas coexistence (with $n = 0, 1, 2, \ldots, 7$, increasing in the direction of the arrow). The constant $\cos\theta_n = 1$ ($\theta_n = 0^{\rm o}$) is marked ∞ and corresponds to two macroscopically separated wall-liquid and liquid-gas interfaces. For every value of η_p^r, the branch corresponding to the lowest $\cos\theta_n$ (i.e. the largest contact angle θ_n) yields the thermodynamically stable state; all other branches are metastable. The crossing point between θ_0 and θ_1 (marked 0-1) denotes the first layering transition and the spinodal point of the 0-layer branch is marked 0'. Also indicated is the location of the wetting transition (star) according to Brader et al. [30, 31].

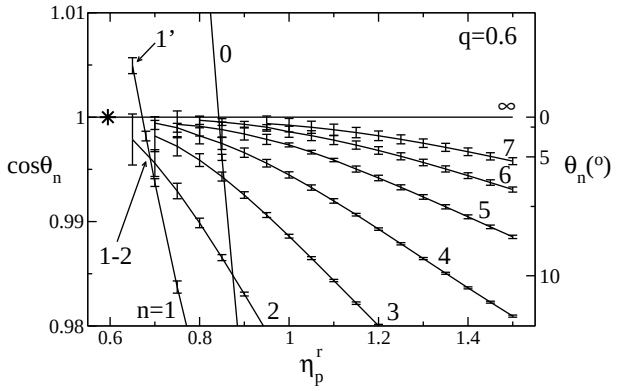

FIG. 4: Same as Fig. 3, but magnified close to $\cos\theta_n = 1$. For the sake of clarity, some of the points of the 3-, 4- and 5-layer branches close to the wetting transition are omitted. Indicated is the location of the second layering transition (marked 1-2) and the 1-layer spinodal point (1').

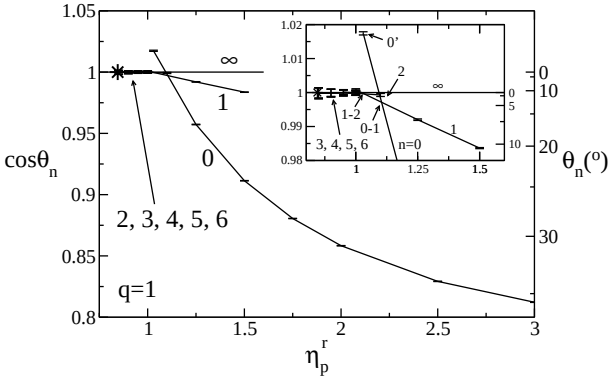

FIG. 5: Same as Fig. 3, but for $q = 1$. The inset displays a magnification of the area close to the wetting transition. The points marked 0-1 and 1-2 are the first layering and second layering transitions, respectively, and spinodal point of the 0-layer branch is denoted with 0'.

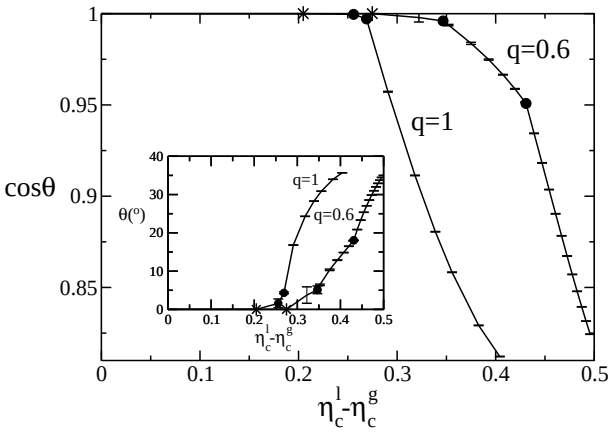

FIG. 6: The equilibrium contact angle, $\cos\theta$ (main figure) and θ (in degrees, displayed in the inset), as a function of the difference in colloid packing fractions, $\eta_c^l - \eta_c^g$, of the coexisting bulk liquid and gas phases for two size ratios, $q = 0.6$ and $q = 1$. The locations of the equilibrium layering transitions are marked by filled circles. The stars are the transitions from partial to complete wetting according to Brader et al. [30, 31].

remarkable fact is that for both size ratios, there is a substantial region in the partial wetting regime close to the wetting transition where the contact angle remains very small, i.e. in the range $(\eta_c^l - \eta_c^g) \approx 0.28 - 0.35$ for $q = 0.6$ and $(\eta_c^l - \eta_c^g) \approx 0.2 - 0.27$ for $q = 1$.

C. Surface phase behaviour

Layering transitions of the AO model at a hard wall were reported earlier by Brader et al. [30, 31] as obtained within the same DFT approximation [28, 29] and using numerical routines similar to those employed in the present work. However, in contrast to the present study, Brader et al. determined (implicitly) spinodal points along two paths: First, by reducing η_p^r at bulk (liquid-gas) coexistence and following the evolution of the 0-layer state, observing jumps to 1-layer and subsequently higher-layer states, and second, by keeping η_p^r fixed and approaching the gas branch of the binodal by increasing η_c, starting from very small values. Results along reversed paths for the second case, i.e. decreasing μ_c at constant η_p^r, were taken to ascertain that hysteresis effects are small, and it was concluded that the spinodal points give reasonable indications of the locations of the equilibrium layering transitions [31, 44]. We will discuss in the following the relation of these findings to those of the present work. For this purpose, we have chosen a reference case, i.e. the first layering transition for $q = 1$, and mapped out its surface phase behaviour completely, i.e. including binodal and spinodal lines off-bulk coexistence. The result is plotted in Fig. 7.

The layering transition binodal is obtained by determining, for each value of η_p^r, the value of η_c at which the 0-layer and 1-layer states have equal interface tensions and are thus in thermodynamic coexistence. The resulting binodal line extends below the first layering transition at bulk coexistence, at $\eta_{p,0-1}^r \approx 1.1$, to lower values of η_p^r into the bulk gas phase region. As this is a transition between two (surface) phases of the same symmetry, a van-der-Waals loop in the free energy and a critical point are mandatory. In order to find the location of the critical point, we fit our data for the colloid adsorption $\Gamma_c(\eta_p^r)$ of the coexisting 0-layer and 1-layer states with a fourth-order polynomial, $\eta_p^r = a_0 + a_2(\Gamma_c - a_1)^2 + a_3(\Gamma_c - a_1)^3 + a_4(\Gamma_c - a_1)^4$, where the a_i are free fit parameters, see Fig. 7. The value of a_0 is an estimate of the critical value of η_p^r, and the functional form is chosen to yield the mean-field critical exponent of 1/2, i.e. $(\Gamma_c - a_1) \sim (\eta_p^r - a_0)^{1/2}$, as the DFT is a mean-field theory in the sense that it does not capture fluctuation effects. The accuracy in colloid packing fraction η_c of points on the layering binodal is high; typically smaller than 0.1% of η_c. However, the critical point is an extrapolation and is therefore much more sensitive to errors, i.e. these may be as large as 3% in η_p^r and 1% in η_c. We have also located the 0-layer spinodal by taking paths at constant η_p^r and increasing values of η_c monitoring the stability of the solution under the iteration procedure. The values of η_c where the 0-layer state becomes unstable and converges to the 1-layer state defines the "adsorption spinodal", located at *larger* values at η_c compared to the layering binodal. (The precise location of spinodal points is subject to the numerical resolution of the step size in η_c, i.e. typically 1% in η_c.) Similarly, we have investigated the stability of the 1-layer states upon reducing η_c at constant η_p^r. This defines the "desorption spinodal", where the 1-layer solutions converge to the 0-layer states and which is located at *smaller* values of η_c as compared to the layering binodal. Upon decreasing η_p^r, both spinodals and the layering binodal end at the surface critical point. Indeed even for values of η_p^r quite above the layering critical point the adsorption and desorption spinodals are very close and we can confirm the finding of Brader et

al. that hysteresis effects at constant η_p^r are small.

Next, we discuss the various aspects of this surface phase transition in relation to bulk liquid-gas coexistence. We first note that no intrinsic difference is observed between the layering phase transition in the stable gas region and that in the two-phase region where the gas is metastable. In the following, we consider the three different surface phase transition lines, i.e. the adsorption spinodal, layering binodal and desorption spinodal, and their relation to the bulk binodal. First, the crossing point of the adsorption spinodal and the bulk liquid-gas binodal denotes the spinodal point terminating the metastability region of the 0-layer state upon reducing η_p^r at bulk coexistence. This corresponds to the adsorption spinodal point of the contact angle (see Fig. 5), as located previously by Brader et al. (as well as other adsorption spinodal points at bulk coexistence for different size ratios, $q = 0.6, 0.7, 1$). Our numerical value of η_p^r agrees well with that of Ref. [31]. Second, the crossing point between layering binodal and bulk binodal is the layering transition at bulk coexistence (accompanied by a kink in the contact angle, as outlined above). This statepoint can be seen as a triple point between the bulk liquid and two different surface states of the bulk gas. The location of this triple point is quite different from the adsorption spinodal point at bulk coexistence. Although hysteresis for a path at constant η_p^r is small, this is not the case for the path along bulk coexistence, due to the fact that the gas branch of the bulk binodal and the layering (spinodal and binodal) lines have very similar slopes. Hence the location of any crossing point is very sensitive to the precise location of the individual lines. Third, in striking contrast to the previous two cases, the desorption spinodal *does not* cross the bulk binodal, but remains in the one-phase gas region for increasing values of η_p^r. We have checked this for one additional path at $\eta_p^r = 2$, starting with a 1-layer profile at bulk coexistence and decreasing η_c and indeed found the desorption spinodal point in the one-phase gas region. This behaviour is consistent with the behaviour of the contact angle, which we discussed above for $q = 0.6$ and $q = 1$, and where adsorption spinodal points were found upon decreasing η_p^r, but no desorption spinodal points were found upon increasing η_p^r. Although we have determined this scenario only extensively for the first layering transition for $q = 1$, we believe it to hold more generally for higher layering transitions and other size ratios.

In order to summarize our present results and those of Ref. [31] for the layering transitions of the AO model at a hard wall, we draw the surface phase diagram for $q = 1$ in Fig. 8. The results for the n-layer adsorption spinodal points for $n = 0, 1, 2, 3$ at bulk coexistence are taken from Ref. [31]. At bulk coexistence, the first and the second layering binodal points are located at higher fugacities compared to the corresponding 0-layer and 1-layer adsorption spinodal points, respectively. Higher layering transitions, corresponding to 2- and 3-layer spinodal points of Brader et al. do not emerge from our present data. On the other hand, Brader et al. have not found layering lines extending into the bulk gas phase for $q = 1$ and which we have located for the first layering transition. We have not searched for a similar layering line in case of the second layering transition. However, from the topology of the first layering transition, which we established above, and taking into account the considerable separation of the second layering binodal and the 1-layer adsorption spinodal points at bulk coexistence, it seems plausible that such a layering binodal line also exists for the second layering transition.

Next, we compare our results to those from simulations by Dijkstra and van Roij for $q = 1$ [21]. They find different regimes of complete and partial wetting, and first, second and third layering transitions located off-bulk coexistence. Our results for the first layering binodal line extending into the one-phase gas region are in qualitative agreement with their findings. Previous comparisons with DFT results [31] left a puzzle because a layering line was found for $q = 0.6$, but not for $q = 1$. The length of this first layering binodal line obtained from DFT is considerably larger (in range of η_p^r) than that found in simulations [21]. With hindsight, this deviation seems consistent with that in other situations, as too small values for the critical polymer fugacities compared to simulations are also found in bulk (see e.g. [23]) or in confinement in planar capillaries [45, 46]. We have not obtained results for the higher-n layering binodal lines, so we can not compare the DFT for $n > 1$ efficiently with simulations. Nevertheless, the overall agreement is good and the DFT seems to capture all relevant effects: i.e. the layering transitions at bulk coexistence, a layering line extending into the one-phase region and a wetting transition [31]. Given the approximate nature of the free energy functional and the fact that the surface phase transitions are governed by tiny free energy differences, this is quite remarkable.

Coming back to $q = 0.6$, we summarize our results and that of Brader et al. [30, 31] in Fig. 9. Similar to the case of $q = 1$, the first and second layering transitions at bulk coexistence are located at higher fugacities than the corresponding 0-layer and 1-layer adsorption spinodal points, respectively. The effect, however, is more dramatic than for $q = 1$, cf. Fig. 8. Brader et al. have also found a 2-layer adsorption spinodal point, indicating the existence of a third layering transition, whose binodal we have not been able to locate. We have also determined the first layering line extending into the bulk gas phase and find it to be remarkably long. The location of the critical point is determined with the same fit procedure as described above for the first layering transition for $q = 1$. The large separation along the bulk binodal of the second layering transition and the 1-layer adsorption spinodal point suggests again the presence of a second layering line.

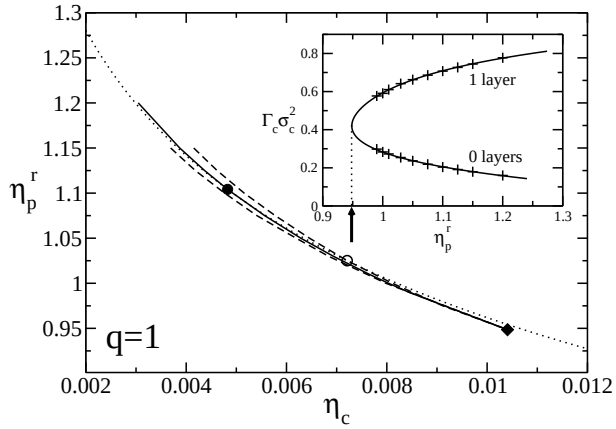

FIG. 7: The full surface phase diagram of the first layering transition (from the 0-layer to the 1-layer state) for $q = 1$ as a function of (bulk) colloid packing fraction, η_c, and polymer reservoir packing fraction, η_p^r. Shown is the layering binodal (full line), the 1-layer desorption spinodal (dashed line, left), 0-layer adsorption spinodal (dashed line, right), and the gas branch of the bulk liquid-gas binodal (dotted line). The point where the layering binodal crosses the bulk liquid-gas binodal is the first layering transition at bulk coexistence (filled circle). The point where the 0-layer adsorption spinodal line hits the bulk binodal is the 0-layer spinodal point at bulk coexistence (open circle), according to Brader et al. [31]. Both spinodals and the binodal terminate at the layering critical point (filled diamond) located off-bulk coexistence in the one-phase gas region. Note that the 1-layer desorption spinodal runs entirely in the one-phase gas region and hence does not cross the bulk binodal. The inset shows the colloid adsorption, $\Gamma_c\sigma_c^2$, of the coexisting 0-layer and 1-layer states (along the layering binodal) as a function of polymer reservoir packing fraction, η_p^r; the dividing surface is chosen at $z = \sigma_c/2$ (lower bound of the integral in Eq. 6). The symbols are obtained from DFT, the full line is the fit (see text) and the arrow at the horizontal axis denotes the estimated value of η_p^r at the layering critical point.

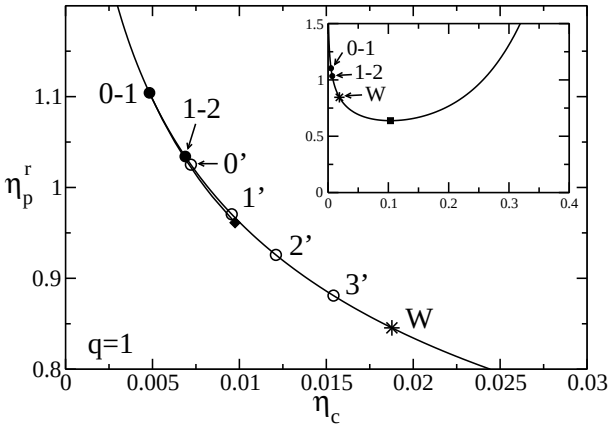

FIG. 8: Summary of the known features of the surface phase diagram of the AO model at a hard wall for size ratio $q = 1$ as a function of colloid packing fraction, η_c, and polymer reservoir packing fraction, η_p^r. Shown are the gas branch of the bulk binodal (full line), equilibrium first (filled circle, marked 0-1) and second (filled circle, marked 1-2) layering transitions at bulk coexistence, as obtained from the present work. The first layering critical point (diamond) is connected via the layering binodal line (full curve) to the first layering transition at bulk coexistence. The spinodal lines are omitted for clarity. The 0-, 1-, 2-, 3-layer adsorption spinodal points at bulk coexistence (open circles, marked $0'$, $1'$, $2'$ and $3'$ respectively) and the wetting transition (star, marked W) are taken from Refs. [31]). The inset shows part of the data together with the bulk critical point (large filled square) on a larger scale.

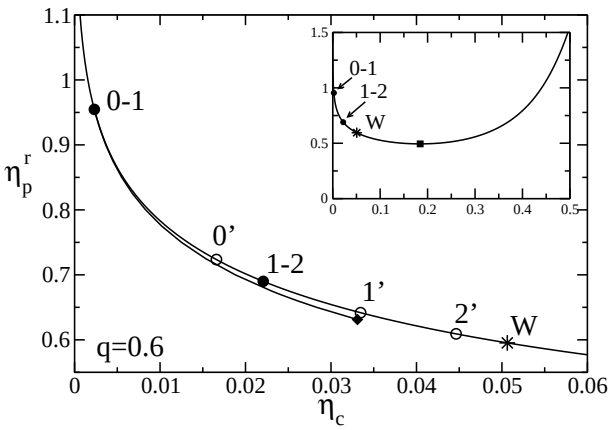

FIG. 9: Same as Fig. 8 but for $q = 0.6$. The 0-layer adsorption spinodal [30, 31] connecting statepoint $0'$ with the surface critical point (diamond) is omitted for clarity.

V. CONCLUSION

In conclusion, we have investigated the contact angle, θ, of the (colloidal) liquid-gas interface and a hard wall using the AO model colloid-polymer mixture and considering two different polymer-to-colloid size ratios, $q = 0.6$ and $q = 1$. Our results for θ are obtained via Young's equation from independent numerical DFT calculations of the liquid-gas, the wall-gas, and the wall-liquid interfacial free energies at bulk coexistence. At the planar wall-gas interface at bulk coexistence, we identify a range of different metastable states each corresponding to a number of adsorbed colloid layers at the wall. We argue that the globally stable state corresponds to the lowest wall-gas interface tension, and therefore possesses the largest value of θ. For small density differences of the coexisting liquid and gas, i.e. close to the bulk critical point, the wall is completely wet by colloidal liquid [30, 31] and hence, $\theta = 0$. Moving along bulk coexistence, away from the critical point, the wetting transition [30, 31] is crossed, and θ becomes non-zero. However, typical values of θ remain very small in a considerable range of statepoints in the partial wetting regime. Mediated by a sequence of first-order layering transitions at the wall-gas interface, the contact angle grows upon moving further from the critical point and reaches typical values up to $\sim 35^o$. These layering transitions of the coexisting colloidal gas in contact with the wall appear as a discontinuities in

the slope of θ as a function of a thermodynamic control parameter, e.g. the polymer reservoir packing fraction or the colloid packing fraction difference between both coexisting bulk phases.

Previous difficulties to measure the contact angle accurately [7] have been overcome by Aarts and Lekkerkerker with the use of confocal scanning laser microscopy [9] in a system with $q = 0.56$. The authors conclude that $\theta = 0$ for all statepoints considered, consistent with their direct observation of a prominent colloid wetting film at the interface of the bulk gas with the wall. They point out that actual values of θ are very sensitive to the precise determination of the location of the wall. Large values of contact angles as well as the observation of the transition to complete wetting have been reported by Wijting et al. [10, 11], using extrapolation of dynamical measurements (i.e. moving the wall) to zero velocity. However, some reservations have been made with respect to the latter results [9]. The magnitude of the contact angle results from subtle differences between the interface tensions and we do not expect our present results to resolve experimental issues. The contact angles which we have calculated for the highly idealized AO model in contact with a hard wall can therefore only serve as a reference case. Important effects due to more realistic polymer-polymer interactions [34], polydispersity and gravity are not captured in our present model (see Ref. [31] for a discussion).

We have also reconsidered the surface phase behavior of the AO model colloid-polymer mixture at a hard wall. This system is known to exhibit a sequence of first-order layering transitions upon following the gas branch of the liquid-gas bulk binodal towards the bulk critical point (i.e. reducing η_p^r). In addition, layering lines extending off-bulk coexistence into the one-phase gas region have been located. Such a layering transition is characterized by a jump in the colloid adsorption at the wall and can be identified as the growth of an additional colloid layer at the wall-gas interface [21, 30, 31]. For one specific case, being the first layering transition for size ratio $q = 1$, we have determined the layering binodal, which gives the equilibrium location of the transition, to high accuracy. In addition, we have located the 0-layer adsorption spinodal line, beyond which (for higher η_c at constant η_p^r) the 0-layer state is unstable and the 1-layer desorption spinodal line, marking the end of stability of the 1-layer state (i.e. for lower η_c at constant η_p^r). The layering binodal and the adsorption and desorption spinodal lines end at a critical point, located in the single-phase gas region of the bulk phase diagram. The crossing point of the layering binodal and the bulk binodal represents a triple point between the bulk liquid and the two layered states (0 and 1 layers) of the bulk gas which have different values of the adsorption of both components. We find the location of this triple point to differ substantially from the (previously identified [30, 31]) crossing point of the adsorption spinodal and the bulk binodal. Remarkably, we could not find a crossing point of the desorption spinodal and the bulk binodal and its absence gives rise to continued (meta)stability of the 1-layer state upon increasing η_p^r at coexistence. We believe that this scenario holds for higher layering transitions and other size ratios. We have presented further results for the second layering transition for $q = 1$ as well as for first and second layering transitions for $q = 0.6$. The order of the wetting transition and whether it occurs via an infinite or a finite sequence of layering transitions remain open questions. Whether the occurrence of layering transitions is specific to the AO model (see also Ref. [31] for a more extensive discussion) or would be present in more realistic descriptions of colloid-polymer mixtures, is another interesting question. However, any experimental attempt to reveal such (layering) phase behavior would require exceptional accuracy for determining θ or resolution on the particle level for direct observation.

Acknowledgments

D. G. A. L. Aarts is thanked for pointing out the relevance of the wall contact angle of the colloidal liquid-gas interface to us. We acknowledge useful discussions and correspondence with R. Evans, J. M. Brader, and R. Roth. R. Evans is also thanked for critically reading of what turned out to be a preliminary version of our manuscript and R. Roth for an independent check of numerical results. This work is financially supported by the SFB-TR6 program "Physics of colloidal dispersions in external fields" of the *Deutsche Forschungsgemeinschaft* (DFG). The work of MS is part of the research program of the *Stichting voor Fundamenteel Onderzoek der Materie* (FOM), that is financially supported by the *Nederlandse Organisatie voor Wetenschappelijk Onderzoek* (NWO).

[1] W. C. K. Poon. *J. Phys.: Cond. Matt.*, 14:R859, 2002.
[2] H. Löwen. *J. Phys.: Cond. Matt.*, 13:R415, 2001.
[3] E. H. A. de Hoog and H. N. W. Lekkerkerker. *J. Phys. Chem. B*, 103:5274, 1999.
[4] E. H. A. de Hoog, H. N. W. Lekkerkerker, J. Schulz, and G. H. Findenegg. *J. Phys. Chem. B*, 103:10657, 1999.
[5] B.-H. Chen, B. Payandeh, and M. Robert. *Phys. Rev. E*, 62:2369, 2000.
[6] B.-H. Chen, B. Payandeh, and M. Robert. *Phys. Rev. E*, 64:042401, 2001.
[7] D. G. A. L. Aarts, J. H. van der Wiel, and H. N. W. Lekkerkerker. *J. Phys.: Cond. Matt.*, 15:S245, 2003.
[8] D. G. A. L. Aarts, M. Schmidt, and H. N. W. Lekkerkerker. to appear in Science.
[9] D. G. A. L. Aarts and H. N. W. Lekkerkerker. submitted to *J. Phys.: Cond. Matt.* (Proceedings of the CODEF

conference 2004).
[10] W. K. Wijting, N. A. M. Besseling, and M. A. Cohen Stuart. *Phys. Rev. Lett.*, 90:196101, 2003.
[11] W. K. Wijting, N. A. M. Besseling, and M. A. Cohen Stuart. *J. Phys. Chem. B*, 107:10565, 2003.
[12] S. Asakura and F. Oosawa. *J. Chem. Phys.*, 22:1255, 1954.
[13] S. Asakura and F. Oosawa. *J. Polym. Sci.*, 33:183, 1958.
[14] A. Vrij. *Pure and Appl. Chem.*, 48:471, 1976.
[15] A. P. Gast, C. K. Hall, and W. B. Russell. *J. Coll. Int. Sci.*, 96:251, 1983.
[16] H. N. W. Lekkerkerker, W. C. K. Poon, P. N. Pusey, A. Stroobants, and P. B. Warren. *Europhys. Lett.*, 20:559, 1992.
[17] E. J. Meijer and D. Frenkel. *Phys. Rev. Lett.*, 67:1110, 1991.
[18] E. J. Meijer and D. Frenkel. *J. Chem. Phys.*, 100:6873, 1994.
[19] M. Dijkstra, J. M. Brader, and R. Evans. *J. Phys.: Cond. Matt.*, 11:10079, 1999.
[20] P. G. Bolhuis, A. A. Louis, and J.-P. Hansen. *Phys. Rev. Lett.*, 89:128302, 2002.
[21] M. Dijkstra and R. van Roij. *Phys. Rev. Lett.*, 89:208303, 2002.
[22] R. L. C. Vink and J. Horbach. *Preprint*, cond-mat/0310404.
[23] R. L. C. Vink and J. Horbach. submitted to *J. Phys.: Cond. Matter*. (Proceedings of the CODEF conference).
[24] J. Dzubiella, A. Jusufi, C. N. Likos, C. von Ferber, H. Löwen, J. Stellbrink, J. Allgaier, D. Richter, A. B. Schofeld, P. A. Smith, W. C. K. Poon, and P. N. Pusey. *Phys. Rev. E*, 64:010401, 2001.
[25] A. Vrij. *Physica A*, 235:120, 1997.
[26] J. M. Brader and R. Evans. *Europhys. Lett.*, 49:678, 2000.
[27] J. M. Brader, M. Dijkstra, and R. Evans. *Phys. Rev. E*, 63:041405, 2001.
[28] M. Schmidt, H. Löwen, J. M. Brader, and R. Evans. *Phys. Rev. Lett.*, 85:1934, 2000.
[29] M. Schmidt, H. Löwen, J. M. Brader, and R. Evans. *J. Phys.: Cond. Matt.*, 14:9353, 2002.
[30] J. M. Brader, R. Evans, M. Schmidt, and H. Löwen. *J. Phys.: Cond. Matt.*, 14:L1, 2002.
[31] J. M. Brader, R. Evans, and M. Schmidt. *Mol. Phys.*, 101:3349, 2003.
[32] P. P. F. Wessels, M. Schmidt, and H. Löwen. *J. Phys.: Cond. Matt.*, 16:L1, 2004.
[33] A. Fortini et al. in preparation.
[34] D. G. A. L. Aarts, R. P. A. Dullens, H. N. W. Lekkerkerker, D. Bonn, and R. van Roij. *J. Chem. Phys.*, 120:1973, 2004.
[35] J. S. Rowlinson and B. Widom. *Molecular Theory of Capillarity*. Dover Publications Inc., Mineola, New York, 1st edition, 2002.
[36] D. E. Sullivan and M. M. Telo da Gama. Wetting transitions and multilayer adsorption at fluid interfaces. In C. A. Croxton, editor, *Fluid Interfacial Phenomena*, page 45. John Wiley & Sons Ltd, 1986.
[37] S. Dietrich. Wetting phenomena. In C. Domb and J. L. Lebowitz, editors, *Phase Transitions and Critical Phenomena*, volume 12, page 1. Academic Press, London, 1988.
[38] R. Evans. Chapter 3, density functionals in the theory of nonuniform fluids. In D. Henderson, editor, *Fundamentals of Inhomogeneous Fluids*, page 85. Dekker, New York, 1992.
[39] A. A. Broyles. *J. Chem. Phys.*, 33:456, 1960.
[40] R. Evans, J. R. Henderson, D. C. Hoyle, A. O. Parry, and Z. A. Sabeur. *Mol. Phys.*, 80:755, 1993.
[41] R. Evans, R. J. F. Leote de Carvalho, J. R. Henderson, and D. C. Hoyle. *J. Chem. Phys.*, 100:591, 1994.
[42] J. R. Henderson. *Phys. Rev. E*, 50:4836, 1994.
[43] M. Schmidt, M. Dijkstra, and J. P. Hansen. unpublished.
[44] J. M. Brader and R. Evans. private communication.
[45] M. Schmidt., A. Fortini, and M. Dijkstra. *J. Phys.: Cond. Matter*, 48:S3411, 2003.
[46] M. Schmidt, M. Dijkstra, and J. P. Hansen. submitted to *J. Phys.: Cond. Matt.* (Proceedings of the CODEF conference 2004).
[47] We do not include the tensorial weight function in the present calculations.
[48] The reported jump in γ_{wg} as a function of difference in colloid packing fractions in the liquid and gas phases at the first layering transition [32] arises from crossing the adsorption spinodal rather than the binodal. The equilibrium curve for γ_{wg} is continuous.